CHALMERS
UNIVERSITY OF TECHNOLOGY

3D-Printed Antireflection Structures for Enhanced Transmission in the 30–50 GHz Range

Downloaded from: https://research.chalmers.se, 2026-11-17 04:30 UTC

Citation for the original published paper (version of record):
Shilinkov, I., Chernikov, V., Helldner, L. et al (2025). 3D-Printed Antireflection Structures for Enhanced Transmission in the 30–50 GHz Range. 34th IEEE International Symposium on Space THz Technology

N.B. When citing this work, cite the original published paper.

© 2025 IEEE. Personal use of this material is permitted. Permission from IEEE must be obtained for all other uses, in any current or future media, including reprinting/republishing this material for advertising or promotional purposes, or reuse of any copyrighted component of this work in other works.

(article starts on next page)

3D-Printed Antireflection Structures for Enhanced Transmission in the 30–50 GHz Range

Iaroslav Shilinkov[1], Viktor Chernikov[1], Leif Helldner[2], Igor Lapkin[2], Denis Meledin[2], Vincent Desmaris[2], Victor Belitsky[2], and François Joint[2*]

***Abstract*— We present a scale-model investigation of a novel, two-layer antireflection (AR) metamaterial intended for future 211–373 GHz (ALMA Bands 6 & 7) vacuum windows and cryogenic IR filters. To verify the concept rapidly and cost-effectively, the design was down-scaled to the 30–50 GHz band and fabricated in polypropylene on a commercial 3-D printer. Analytical quarter-wave transformer theory set the target impedances. These were done with a square unit-cell that alternates circular posts and complementary holes to obtain the required effective permittivity. Full-wave Floquet-periodic simulations predict < –20 dB reflection across the bandwidth. Quasi-optical measurements of the printed AR structure confirm that wide-band impedance matching can be achieved with entirely additively-manufactured polymer layers, which opens up-scaling the same topology to large-aperture windows for millimetre- and sub-millimetre-wave instruments in radioastronomy.**

***Keywords*—3D Printing, Anti-reflection Coating, Millimeter-wave, Quasi-optics.**

I. Introduction

MINIMISING Fresnel reflections at dielectric boundaries is essential in millimetre- and sub-millimetre-wave receivers, where every tenth-of-a-decibel of extra loss degrades detector noise temperature and instrument mapping speed. Nowhere is this more critical than in the vacuum window, the first optical element seen by the incoming beam. Large astronomical cryostats such as those on ALMA must combine diameters ≥80 mm with one-bar pressure integrity, making the window simultaneously an optical component and a load-bearing mechanical membrane. Even when low-loss polymers such as ultra-high-molecular-weight polyethylene (UHMW-PE) are employed, the unstructured surfaces still produce Fresnel reflections that degrade receiver sensitivity; an efficient AR structure therefore remains essential for wide-band instruments.

Classical broadband AR solutions such as multilayer thin-films, diced or laser-textured sub-wavelength structures, and deep triangular grooves[1–3]—can reach return losses below –20 dB, but they rely on specialised clean-room or five-axis machining and become increasingly costly as the aperture grows or the target wavelength shortens. Moreover, fabricating such structures on curved or double-sided geometries pushes conventional tooling close to its practical limits.

Recent progress in additive manufacturing has opened an alternative path: low-cost 3-D printers can now reproduce features below 100 µm with polymers whose dielectric loss is tolerable up to hundreds of gigahertz. This capability has already enabled millimetre-wave lenses and feed-horns for ALMA Band 1 (35–52 GHz) and other instruments[4], but to date no additive workflow has been demonstrated for large-aperture vacuum windows with engineered impedance matching.

Here we report the first step toward that goal. We design a two-layer quarter-wave metamaterial, implemented as a square lattice of complementary circular posts and holes, that realises a maximally flat transformer between free space and bulk polymer. To verify the concept rapidly and inexpensively we scale the geometry to 30–50 GHz and print 75 mm diameter vacuum windows in polypropylene (PP) on a commercial fused-filament printer. Analytical impedance theory predicts < –20 dB reflection across the 50 % fractional bandwidth; Floquet-periodic finite-element simulations and quasi-optical measurements confirm the calculation within 0.03 dB.

The successful scale test demonstrates that additive manufacturing can deliver the required electromagnetic accuracy and surface quality. Following with these results we are now transferring the lattice to higher frequencies and will evaluate it at the full 211–373 GHz span of ALMA Bands 6 & 7 in a vacuum window. If successful, the approach promises a fast, scalable route to broadband, low-loss cryogenic windows and filters for the next generation of millimetre-wave telescopes.

II. Theory: Two-Section Maximally-Flat Quarter-Wave Transformer

The analytical design follows the binomial (maximally flat) impedance-matching rules[5,6]. For a two-section quarter-wave transformer ($N = 2$) that matches free space ($Z_0 = 376.99\ \Omega$) to a dielectric load, Z_L, the characteristic impedances are $Z_1 = Z_0.R^{1/4}$ and $Z_2 = Z_0.R^{3/4}$ where $R = Z_L/Z_0$. With $\varepsilon_r = 2.85$ for PP, the load impedance is $Z_L = Z_0/\sqrt{\varepsilon_r} = 217.6\ \Omega$,

[1]Department of Electrical Engineering, Chalmers University of Technology, Gothenburg, Sweden; [2]Group for Advanced Receiver Development, Onsala Space Observatory, Department of Space, Earth and Environmental Sciences, Chalmers University of Technology, Gothenburg, SE-41296, Sweden. *Corresponding author (email: joint@chalmers.se).

NOTES:

yielding $Z_1 \approx 328\,\Omega$ and $Z_2 \approx 250\,\Omega$ at the mid-band frequency $f_0 = 40$ GHz. Each layer is one quarter wavelength long inside its own effective medium, so the physical thicknesses become $t_1 = \lambda_0/(4\sqrt{\varepsilon_{eff,1}}) \approx 1.31$ mm and $t_2 \approx 1.10$ mm.

The maximally flat response suppresses the first derivative of the reflection coefficient at f_0 producing a -20 dB return-loss bandwidth of roughly 30-50 GHz ($\approx 50\%$ fractional) as shown in Fig. 1 which was calculated for polypropylene (PP) with $\varepsilon_{r,PP} = 2.85$ and $\tan(\delta) = 10^{-2}$.

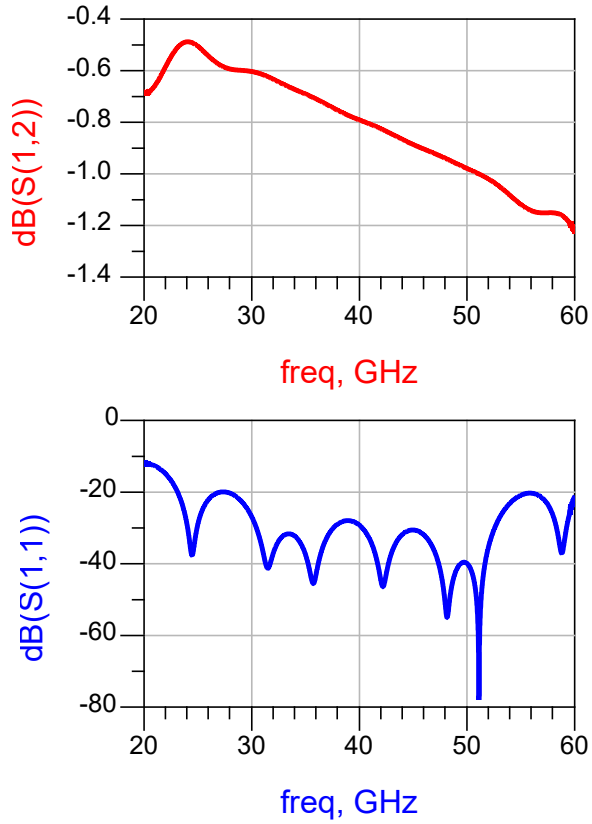

Fig 1. Calculated scattering parameters for the back-to-back two-section quarter-wave transformer. Top panel: power transmission $|S_{21}|$ across the 30–50 GHz design band calculated for PP $\tan(\delta) = 10^{-2}$. Bottom panel: power reflection remains below –20 dB over the same range.

III. METAMATERIAL UNIT-CELL DESIGN

The antireflection coating is implemented as a bi-layer square lattice whose effective permittivities reproduce the impedances derived above. We assume an isotropic binary mixture of PP ($\varepsilon_r \approx 2.85$ at 40 GHz) and air; when the lattice pitch p and feature diameter d satisfy $p, d \ll \lambda_{min}/10$ where ($\lambda_{min} = 6\,mm$ at 50 GHz), the layer can be treated as a uniform dielectric with

$$\varepsilon_{eff} = \frac{\varepsilon_{r,PP} V_{PP} + V_{air}}{V_{total}} \tag{1}$$

From the previously calculated Z_1 and Z_2, the required permittivities $\varepsilon_{eff,1} \approx 1.32$ and $\varepsilon_{eff,2} \approx 2.28$ which translate to polymer volume fractions $f_1 \approx 0.18$ and $f_2 \approx 0.71$. For a square unit cell containing either a circular hole (radius R_h) or a circular post (radius R_p) the air-to-polymer fill fraction is linked to ε_{eff} by the volume-weighted mixing rule:

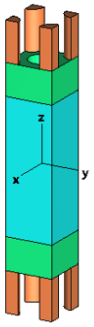

Fig 2. Finite-element model of the bilayer antireflection window. The structure is treated as an infinite two-dimensional lattice, so the simulation domain is reduced to a single square unit cell bounded by master–slave (periodic) walls.

$$\varepsilon_{eff} = \varepsilon_{r,PP}\left(1 - \frac{\pi R^2}{a^2}\right) + \frac{\pi R^2}{a^2} \tag{2}$$

which rearranges to the compact design formulas:

$$R_h = a\sqrt{\frac{\varepsilon_{r,PP} - \varepsilon_{eff}}{\pi(\varepsilon_{r,PP} - 1)}} \tag{3}$$

$$R_p = a\sqrt{\frac{\varepsilon_{eff} - 1}{\pi(\varepsilon_{r,PP} - 1)}} \tag{4}$$

Which gives $R_h = 1.16$ mm for the low-index inner layer (holes) and $R_p = 0.96$ mm for the higher-index outer layer (posts). Both radii remain above the ≈ 0.4 mm feature limit of our 3D printer.

IV. FINITE-ELEMENT METHOD SIMULATIONS

The electromagnetic response was evaluated with ANSYS HFSS using a single unit cell shown in Fig. 2 and excited by dual Floquet ports. This exploits the infinite two-dimensional

NOTES:

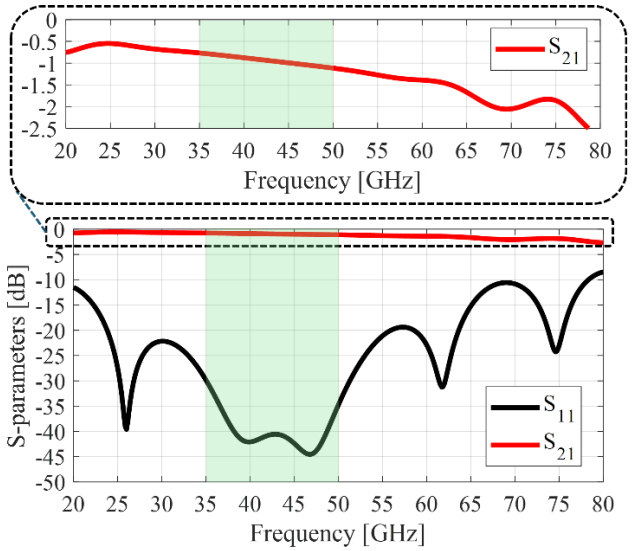

Fig 3. HFSS verification of the back-to-back bilayer antireflection structure, including dielectric loss. The model assigns PP a loss tangent of $\tan(\delta) = 10^{-2}$ at 40 GHz and excites the unit cell with dual Floquet ports.

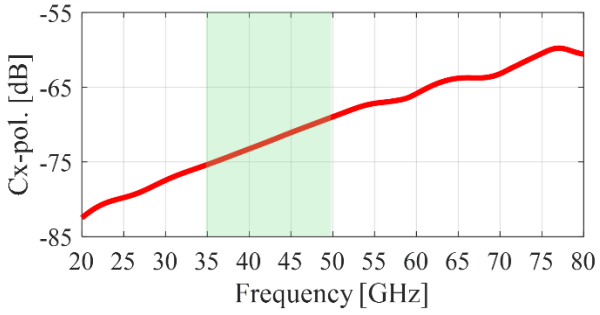

Fig 4. HFSS simulation of the cross-polar performance of the square-symmetric bilayer antireflection structure.

periodicity and allows direct extraction of co- and cross-polar S-parameters with rather low computational cost. The ports launch orthogonal TE_{10} and TM_{01} modes so that co- and cross-polar S-parameters are extracted in one pass. A broadband sweep from 20 GHz to 80 GHz is run with adaptive mesh refinement; The simulated spectra presented in Fig. 3, shows return loss better than 20dB and insertion loss <1dB across the full band. We observe negligible cross-polar coupling (<-55 dB, Fig. 4). This confirms that the pin–hole bilayer meets the 50 % fractional-bandwidth requirement of our scale model and provides a solid foundation for scaling the same topology to the final window operating at 211–373 GHz.

V. MEASUREMENTS

The 30–50 GHz scale model was produced in two identical PP halves, each containing the complete pin–hole bilayer and exactly half of the required bulk thickness. The scale-model coupons were fabricated on a commercial fused-filament machine (Ultimaker 2+) loaded with PP. A 0.25 mm nozzle was selected to resolve the 0.30 mm lands between adjacent posts and holes. Slicing in Cura employed a 250 °C nozzle temperature and a nominal print speed of 30 mm s^{-1}, reduced to 25 mm s^{-1} on the outer perimeter to sharpen feature edges. The extrusion line width was widened to 0.30 mm so neighboring roads merged into fully dense walls. Stringing was suppressed with a 2 mm retraction at 45 mm s^{-1}. The optical micrograph of the 3D printed structure is shown in Fig.5.

The performance of the 3D-printed AR structures was evaluated using a quasi-optical measurement system designed to generate a plane-wave-like beam at the position of the Device Under Test (DUT) (see Fig. 5). The setup included horn antennas optimized for the Q-band (30–50 GHz), connected to a Vector Network Analyzer (VNA) through coaxial-to-rectangular transition. One horn served as the transmitter (Tx), and the other as the receiver (Rx). RF absorbers mitigated parasitic reflections, while polarization grids minimized cross-polarization effects. Only the forward-transmission ($|S_{21}|$) data

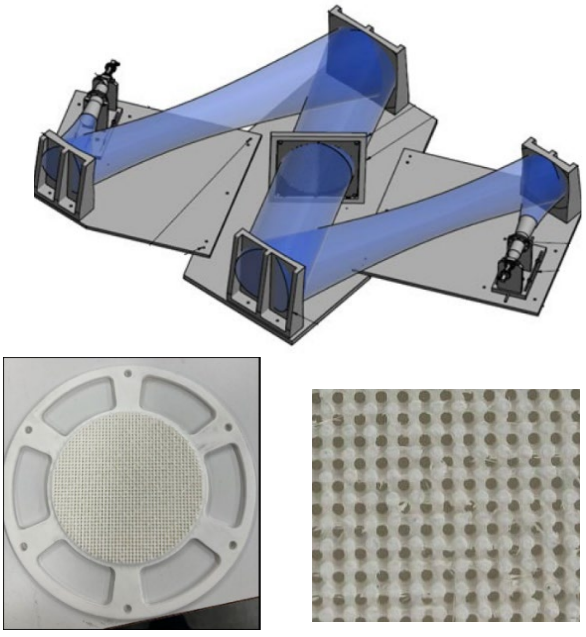

Fig. 5 *(top)* Gaussian-beam telescope used for 30–50 GHz S-parameter tests: two horns and off-axis parabolas focus the beam waist onto the DUT at mid-plane. *(bottom)* Top view of the 3-D-printed PP window; inset shows the bilayer lattice of posts and complementary holes.

NOTES:

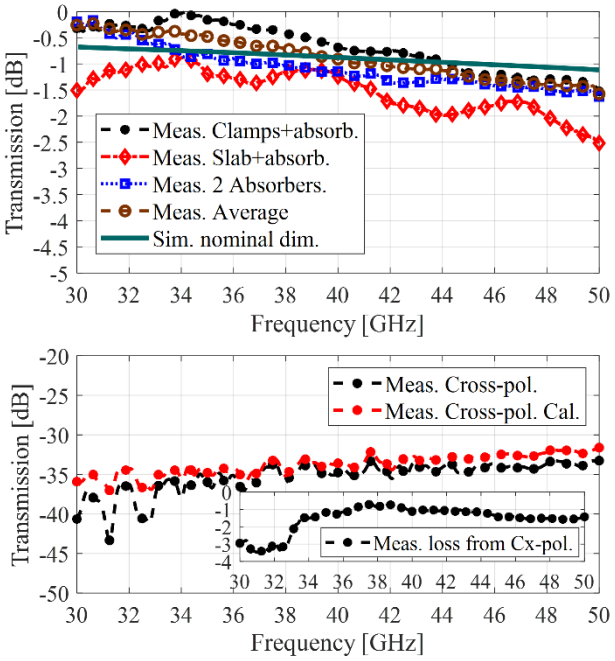

Fig. 6 Experimental S-parameter results for the 3-D-printed bilayer window. *(top)* Co-polar transmission with absorber surrounding the DUT flange. For comparison, the red curve shows an 8 mm polypropylene slab acting as a thin etalon. Adding absorber suppresses edge scattering and reveals the maximally-flat pass-band for the 30–50 GHz design. *(bottom)* Cross-polar transmission.

are reported here. The reflection trace proved unreliable in this quasi-optical bench The experimental results shown in Fig. 6 demonstrated the AR structures' effectiveness in improving transmission efficiency. Comparison with theoretical models validated the performance of the designs and confirmed the feasibility of integrating 3D-printed AR structures into advanced millimeter-wave systems.

VI. Conclusion

A 3-D-printed, two-layer antireflection lattice—scaled to 30–50 GHz—was fabricated in PP and tested as a rapid, low-cost proxy for the planned window prototype at 211–373 GHz. Analytical λ/4-transformer theory ($\varepsilon_{r,\ PP} = 2.85$ and $\tan(\delta) = 10^{-2}$) predicted <–20 dB reflection and <1 dB loss across the band; HFSS Floquet simulations and quasi-optical Tx measurements agree within 0.3 dB, with cross-pol below –35 dB. Printing the structure in two glass-flattened halves produced void-free, dimensionally accurate samples, proving the geometry is manufacturable with off-the-shelf 3D-printing hardware. This scale-model demonstrator validates the lattice at 30–50 GHz and clears the path for our next step: fabricating the same geometry and testing it as a full 211–373 GHz (ALMA Bands 6 & 7) vacuum window. For the full-frequency implementation we will employ advanced lithographic tooling and laser ablation to pattern the sub-wavelength metamaterial directly into UHMW-PE, achieving the necessary feature control below 100 µm.

References

(1) Speirs, P.; Molina, R.; Saenz, E.; Yagoubov, P. M. P.; Murk, A. Design and Measurement of Possible Wide-Band 67-116 GHz ALMA Vacuum Window Anti-Reflection Layers. In *2020 14th European Conference on Antennas and Propagation (EuCAP)*; 2020; pp 1–5. https://doi.org/10.23919/EuCAP48036.2020.9135970.

(2) Yagoubov, P.; Mroczkowski, T.; Belitsky, V.; Cuadrado-Calle, D.; Cuttaia, F.; Fuller, G. A.; Gallego, J.-D.; Gonzalez, A.; Kaneko, K.; Mena, P.; Molina, R.; Nesti, R.; Tapia, V.; Villa, F.; Beltrán, M.; Cavaliere, F.; Ceru, J.; Chesmore, G. E.; Coughlin, K.; Breuck, C. D.; Fredrixon, M.; George, D.; Gibson, H.; Golec, J.; Josaitis, A.; Kemper, F.; Kotiranta, M.; Lapkin, I.; López-Fernández, I.; Marconi, G.; Mariotti, S.; McGenn, W.; McMahon, J.; Murk, A.; Pezzotta, F.; Phillips, N.; Reyes, N.; Ricciardi, S.; Sandri, M.; Strandberg, M.; Terenzi, L.; Testi, L.; Thomas, B.; Uzawa, Y.; Viganò, D.; Wadefalk, N. Wideband 67−116 GHz Receiver Development for ALMA Band 2. *Astron. Astrophys.* **2020**, *634*, A46. https://doi.org/10.1051/0004-6361/201936777.

(3) Schröder, A.; Murk, A.; Yagoubov, P.; Patt, F. Design and Characterization of the ALMA Band 5 Vacuum Window. *IEEE Trans. Terahertz Sci. Technol.* **2016**, *6* (1), 156–162. https://doi.org/10.1109/TTHZ.2015.2497139.

(4) Tapia, V.; Rodríguez, R.; Reyes, N.; Mena, F. P.; Yagoubov, P.; Cuttaia, F.; Bronfman, L. Systematic Study of the Cross Polarization Introduced by Broadband Antireflection Layers at Microwave Frequencies. *Appl. Opt.* **2018**, *57* (31), 9223–9229. https://doi.org/10.1364/AO.57.009223.

(5) Pozar, D. M. *Microwave Engineering*, 4th ed.; Wiley & Sons, Inc.: New Jersey, USA, 2012.

(6) Matthaei, G. L. *Microwave Filters, Impedance-Matching Networks, and Coupling Structures, 1964.*

NOTES: